Available at www.sciencedirect.com

ScienceDirect

journal homepage: www.elsevier.com/locate/watres

Macromolecule mediated transport and retention of *Escherichia coli* O157:H7 in saturated porous media

Hyunjung N. Kim [a], *Sharon L. Walker* [a], *Scott A. Bradford* [b,*]

[a] *Department of Chemical and Environmental Engineering, University of California, Riverside, CA 92521, USA*
[b] *USDA, ARS, US Salinity Laboratory, Riverside, CA 92507, USA*

ARTICLE INFO

Article history:
Received 28 January 2009
Received in revised form
1 September 2009
Accepted 9 September 2009
Available online 12 September 2009

Keywords:
Pathogen
Transport
Escherichia coli O157:H7
Extracellular macromolecules
Polymer bridging
Steric stabilization

ABSTRACT

The role of extracellular macromolecules on *Escherichia coli* O157:H7 transport and retention was investigated in saturated porous media. To compare the relative transport and retention of *E. coli* cells that are macromolecule rich and deficient, macromolecules were partially cleaved using a proteolytic enzyme. Characterization of bacterial cell surfaces, cell aggregation, and experiments in a packed sand column were conducted over a range of ionic strength (IS). The results showed that macromolecule-related interactions contribute to retention of *E. coli* O157:H7 and are strongly linked to solution IS. Under low IS conditions (IS $\leq$ 0.1 mM), partial removal of the macromolecules resulted in a more negative electrophoretic mobility of cells and created more unfavorable conditions for cell–quartz and cell–cell interactions as suggested by Derjaguin-Landau-Verwey-Overbeek (DLVO) interaction energy profiles and cell aggregation kinetics. Consequently, less retention was observed for enzyme treated cells in the corresponding column experiments. In addition, a time-dependent deposition process (i.e., ripening) was observed for untreated cells, but not for treated cells, supporting the fact that the macromolecules enhanced cell–cell interactions. Additional column experiments for untreated cells under favorable conditions (IS $\geq$ 1 mM) showed that a significant amount of the cells were reversibly retained in the column, which contradicts predictions of DLVO theory. Furthermore, a non-monotonic cell retention profile was observed under favorable attachment conditions. These observations indicated that the presence of macromolecules hindered irreversible interactions between the cells and the quartz surface.

Published by Elsevier Ltd.

1. Introduction

Escherichia coli O157:H7, a predominant serotype of enterohemorrhagic *E. coli*, is a Gram-negative pathogenic bacterium. This bacterium can cause severe gastrointestinal disease in humans, such as bloody diarrhea and hemolytic uremic syndrome, which may result in acute renal failure in children (Boyce et al., 1995; Dean-Nystrom et al., 2003; Kaper and Karmali, 2008). More than 70,000 illnesses and 60 deaths per year are estimated to occur in the United States due to *E. coli* O157:H7 infection (Mead et al., 1999).

Pathogens can reach drinking water supplies via a number of pathways; e.g., surface runoff, soil infiltration, and groundwater recharge. The transmission of waterborne diseases by pathogen-contaminated groundwater is a growing concern. An accurate understanding of the transport and fate of pathogens in subsurface and groundwater environments is needed to protect water resources. Much effort has been

* *Corresponding author*. Tel.: +1 951 369 4857; fax: +1 951 342 4964.
E-mail address: scott.bradford@ars.usda.gov (S.A. Bradford).
0043-1354/$ – see front matter Published by Elsevier Ltd.
doi:10.1016/j.watres.2009.09.027

devoted to understand fundamental mechanisms of fate and transport of colloids and microorganisms in porous media (Schijven and Hassanizadeh, 2000; Ginn et al., 2002; Jin and Flury, 2002). The transport and deposition of non-living colloids has frequently been shown to be influenced by physicochemical phenomena between the interacting surfaces (Bradford et al., 2007; Kuznar and Elimelech, 2007; Shen et al., 2007). Unlike the non-living colloids, bacteria are living organisms that exhibit distinct characteristics. For example, bacteria may be rod-shaped and physiologically respond to environmental changes (Frank, 2001; Seltmann and Holst, 2002). Most bacteria possess various types of surface-bound macromolecules such as proteins, lipopolysaccharides, fimbriae, flagella (Frank, 2001; Seltmann and Holst, 2002). In addition, unbound macromolecules (e.g., extracellular polymeric substances) are frequently found outside cell surface (Wingender et al., 1999). These macromolecules have very complex structure, and the type, composition, and amount of macromolecules can vary with other factors, such as bacterial species, nutrient conditions, growth stage, etc. (Law, 2000; Walker et al., 2005; Chen and Walker, 2007).

A growing body of literature indicates that surface/extracellular macromolecules can play a significant role in the interaction of microbes and abiotic surfaces (Kuznar and Elimelech, 2005; Liu et al., 2007; Gargiulo et al., 2007). The presence of macromolecules on/outside the surface of microbes may cause steric forces (Israelachvili, 1992; van Oss, 1994). Several studies reported that surface/extracellular macromolecules can either enhance (Jucker et al., 1998; Rijnaarts et al., 1999; Gargiulo et al., 2007) or hinder (Jucker et al., 1998; Kuznar and Elimelech, 2005, 2006) the adhesion of microbes to abiotic surfaces. Studies have also reported that the presence of bacterial polymeric layers influence cell–cell interactions due to physicochemical (Voloshin and Kaprelyants, 2004) or biological (Frank, 2001; Voloshin and Kaprelyants, 2004) mechanisms. Furthermore, cell–cell interactions have also been proposed to be an important mechanism in bacteria retention in porous media (Bradford et al., 2006b; Kim et al., 2009a), in cell adhesion to biotic/abiotic surfaces (Frank, 2001), and in bacterial colonization/biofilm formation (Frank, 2001; Voloshin and Kaprelyants, 2004). Although much research has been devoted to investigate the macromolecule-mediated interactions (i.e., cell–cell and cell–surface interactions), the fundamental interaction mechanisms are not well understood because the type and extent of the macromolecule-mediated interactions depend on the cell type and the environmental conditions (e.g., pH, IS, temperature). Further study is required to better elucidate these interactions.

E. coli O157:H7 has been reported to produce extracellular polymeric materials, which may protect the cells from harsh environments and initiate cell colonization/biofilm formation (Ryu and Beuchat, 2005; Oh et al., 2007). Previously, we observed that the *E. coli* strain selected for this study produced extracellular materials (Kim et al., 2009b). To directly investigate the influence of macromolecules on the phenotypic properties (e.g., electrophoretic mobility (EPM), hydrophobicity, acid–base property, etc.) of *E. coli* O157:H7 cells some cells were treated with a proteolytic enzyme (i.e., proteinase K) to cleave exposed extracellular macromolecules. The study showed that the presence of the extracellular macromolecules altered the cell surface characteristics and eventually influenced the adhesion behavior of the cells in a batch system at pH = 5.8 (Kim et al., 2009b). Another recent study showed that *E. coli* O157:H7 retention in a packed sand column was inversely proportional to IS under high pH conditions (IS = 1–100 mM and pH = 8.4–9.2) (Kim et al., 2009a). This behavior was not explained by classic DLVO theory (Derjaguin and Landau, 1941; Verwey and Overbeek, 1948). Instead, the trend was attributed to pH-associated steric stabilization (Kim et al., 2009a), indirectly suggesting the presence of potential macromolecule-related interactions.

Although Kim et al. (2009a,b) provide useful insight about the role of extracellular macromolecules on *E. coli* O157:H7 interactions and transport, gaps in knowledge still remain that are addressed in the current work. Specifically, we investigate the potential influence of *E. coli* O157:H7 extracellular macromolecules on: (a) attractive steric interactions under low IS conditions (i.e., polymer bridging); and (b) repulsive steric interactions under low pH conditions (effects are much more subtle at pH = 5.8 than at higher pH conditions). The implications of these steric interactions on cell transport and aggregation is subsequently quantified. For this purpose, a proteolytic enzyme (i.e., proteinase K) was employed to partially cleave the macromolecules on the *E. coli* O157:H7 cell surface, and the transport and retention behavior of the proteinase K treated *E. coli* O157:H7 cells was examined and compared with the untreated cells in a packed sand column over the IS range of 0.01–100 mM KCl (pH 5.8). In addition, aggregation tests were conducted with the untreated and proteinase K treated *E. coli* O157:H7 cells as a function of IS to examine the relationship between cell–cell interaction and cell retention behavior. A similar study has been previously conducted by Kuznar and Elimelech (2006) using *Cryptosporidium parvum* oocysts. They compared the attachment efficiency between untreated and proteinase K treated oocysts to quartz surface in a radial stagnation point flow (RSPF) system. However, the RSPF system only captured irreversible interactions and they focused on repulsive steric interactions. In addition, we are unaware of any other studies that have applied this enzymatic technique for pathogenic *E. coli* O157:H7 in a column system.

2. Materials and methods

2.1. Bacterial growth and preparation

E. coli O157:H7/pGFP strain 72 was obtained from Dr. Pina Fratamico (USDA-ARS-ERRC, Wyndmoor, PA) for this study. The cells were precultured in Tryptic Soy Broth (TSB, Becton Dickinson, Sparks, MD) in the presence of 0.1 g/L ampicillin (Sigma–Aldrich, St. Louis, MO) at 200 rpm and 37 °C in an incubator (Model 4639, Barnstead/Labline, Melrose Park, IL). The precultured cells were transferred onto Tryptic Soy Agar (TSA, Becton Dickinson) in Petri dishes with 0.1 g/L ampicillin (Sigma–Aldrich), and grown for 18 h (stationary phase) at 37 °C. In order to collect the cultured cells, sterile de-ionized (DI) water was added into TSA and the cells were gently scraped using a sterile cell spreader (Fisher Scientific, Fair Lawn, NJ). The collected cells were harvested by centrifugation (Fisher

accuSpin* 3R Centrifuge, Fisher Scientific) for 15 min at 3700 g (Swing Bucket Rotor 7500, Fisher Scientific). The cells were rinsed two additional times using a 10 mM potassium chloride (KCl, Fisher Scientific) solution to remove any remaining growth media, and then resuspended in 3 mL of the same electrolyte solution chemistry of the subsequent experiment. This cell suspension was used to determine cell concentration in a counting chamber (Marienfeld Laboratory Glassware, Germany).

To investigate the role of extracellular macromolecules on *E. coli* O157:H7 transport and retention in a packed sand column, a proteolytic enzyme (proteinase K, Sigma–Aldrich) was employed to partially cleave the extracellular macromolecules from the bacteria. A detailed description of this protocol is available in the literature (Kuznar and Elimelech, 2005; Kim et al., 2009b). Briefly, the untreated cells harvested by the above protocol were suspended into a background solution, which consists of 0.1 mg/mL proteinase K (Sigma–Aldrich), 5 mM EDTA, 0.01 g/L sodium dodecyl sulfate, and 10 mM Tris–HCl (pH 8.0). The final cell concentration was approximately 5×10^8 cells/mL. The cell suspension was incubated at 37 °C and 260 rpm for 3 h to digest macromolecules on/outside the cell surface. The proteinase K treated cells were then rinsed twice with DI water by a centrifugation at 13400 g for 2 min, followed by one more rinsing with DI water at 3700 g for 10 min. All chemicals for the digestion process were reagent grade (Sigma–Aldrich).

2.2. Solution chemistry and bacterial characterization

KCl was selected as the background electrolyte for the *E. coli* O157:H7 characterization and transport experiments, and the IS ranged from 0.01 to 100 mM. The pH for all experiments was maintained at approximately 5.8.

Cell viability, size, and shape were examined as a function of IS for untreated and proteinase K treated *E. coli* O157:H7 cells. Viability tests were performed based on the Live/Dead BacLight (L-7012, Molecular Probes, Eugene, OR) method (Boulos et al., 1999) with an inverted fluorescent microscope (IX70, Olympus, Japan) equipped with a red/green fluorescence filter set (Chroma Technology Corp., Brattleboro, VT). Bacterial cell size and shape were also determined from images taken with the microscope in phase contrast mode. Volume-based equivalent radii and aspect ratios of the cells were determined from the measured lengths and widths of the cells ($n \geq 50$). The percentage of viable cells were determined to be more than 90% regardless of IS and enzyme treatment. The average effective cell diameter was approximately 0.71 μm (minimum and maximum value of 0.66 and 0.78 μm, respectively), and the average aspect ratio also ranged from 2.9 ± 1.6 (minimum) to 3.7 ± 2.2 (maximum). The detailed results for cell viability, size, and shape measurements can be found in Kim et al. (2009b) and indicate that proteinase K did not damage the cell wall during the macromolecule treatment and there was no significant impact of osmotic pressure on *E. coli* O157:H7 cells at low and high IS.

EPM of the untreated and proteinase K treated *E. coli* O157:H7 cells were evaluated as a function of IS (0.01–100 mM). Detailed information regarding the procedures can be found in Kim et al. (2009b). In brief, EPM measurements were conducted at 25 °C using a ZetaPALS analyzer (Brookhaven Instruments Corporation, Holtsville, NY). The pH of the solution was unadjusted. Three different samples were prepared for each solution IS condition and average values of ten runs were obtained for one sample.

Hydrophobicity tests were conducted for the untreated and proteinase K treated *E. coli* O157:H7 cells at 0.01 and 0.1 mM (pH 5.8) based on the microbial adhesion to hydrocarbons (MATH) test (Pembrey et al., 1999). One mL of *n*-dodecane (laboratory grade, Fisher Scientific) was added to 4 mL of a cell suspension, and the suspension was mixed for 2 min. The mixture was then left for at least 15 min at room temperature to allow the two liquids to separate. The percentage of the cells partitioned to the hydrocarbon phase was calculated after the optical density of the cell suspension in the water phase was determined at 546 nm (BioSpec-mini, Shimadzu Corp.). All experiments were conducted at least in triplicate. The results are presented in Table 1. Overall, the proteinase K treated cells were determined to be slightly more hydrophilic than the untreated ones.

Statistical differences between mean values were analyzed using a student *t*-test. When $P < 0.05$, the differences are considered to be statistically significant.

2.3. Cell aggregation tests

In order to evaluate the initial aggregation kinetics of untreated and proteinase K treated *E. coli* O157:H7 cells at different IS, the cells were harvested and washed according to the procedure in Section 2.1. For the untreated cells, the washed pellets were resuspended in the select KCl solution

Table 1 – Electrophoretic mobility of *E. coli* O157:H7 cells as well as the percentage of the cells partitioned into hydrocarbon (*n*-dodecane) before and after proteinase K treatment.[a]

Ionic strength (mM)	Electrophoretic mobility (μm V s^{-1} cm^{-1})[b]		Hydrophobicity (%)	
	Untreated	Proteinase K treated	Untreated	Proteinase K treated
0.01	−1.234 ± 0.135	−3.086 ± 0.265	15.5 ± 2.8	11.3 ± 1.8
0.1	−0.644 ± 0.080	−2.176 ± 0.071	14.5 ± 1.3	11.6 ± 1.7
1	−0.073 ± 0.147	−0.705 ± 0.187	ND	ND
100	−0.112 ± 0.742	−0.053 ± 0.557	ND	ND

a The experiments were conducted at pH 5.8 and at room temperature (22–25 °C).
b Data from Kim et al. (2009b). ND Not determined.

(IS = 0.01, 0.1, 1, and 100 mM) to an optical density (i.e., absorbance value) of 0.6 (dimensionless unit) at a wavelength of 600 nm, which corresponds to the cell concentration of 10^8 cells/mL. The cell suspension (0.4 mL) was transferred into a quartz cuvette (Fisher Scientific) and the upper part of the sample was measured spectroscopically (SP-890, Barnstead International, Dubuque, IA) at the wavelength of 600 nm for 2 h. The aggregation tests for the treated cells were also carried out in the presence of 0.01 and 0.1 mM KCl after the enzyme treatment.

2.4. Porous medium preparation

Ultra-pure quartz sand (Iota® quartz, Unimin Corp., NC), which has the average diameter (d_{50}) of 275 μm, was chosen for column experiments. To remove any metal and organic impurities, the sand was thoroughly cleaned using the method of Litton and Olson (1993). Prior to wet-packing the column, the cleaned sand was re-hydrated by boiling in DI water for 1 h. The total (or effective) porosity was determined to be ca. 0.46 by a gravimetric method. The zeta potential of the quartz sand was measured at IS of 0.01 and 0.1 mM (KCl) using an Electro Kinetic Analyzer (Anton Paar GmbH, Graz, Austria) equipped with a cylindrical cell to calculate DLVO interaction energy between the cells and quartz media. The results for sand zeta potential are provided in Table 2.

2.5. Column experiments

An adjustable length chromatographic column (Omnifit, Boonton, NJ) with a 1.5 cm inner diameter was used for the transport experiments. The column length was adjusted to 10 cm for all experiments. More than 10 pore volumes (PV) of DI water was pumped through the column using a syringe pump (KD Scientific Inc., New Hope, PA), followed by at least 10 PV of the electrolyte at the selected IS to equilibrate the column. A 4 PV pulse of the cell suspension with a concentration of ca. 5×10^8 cells/mL was injected, followed by a bacteria-free electrolyte solution (>20 PV). If needed, flow interruption and low IS solution (i.e., DI water) flush tests were conducted when the effluent cell concentration was close to baseline (ca. zero). The Darcy velocity of the system was maintained at 0.1 cm/min, and the corresponding Reynolds number and Peclet number values were 9.8×10^{-3} and 5.3×10^{-3}, respectively. The effluent concentration of *E. coli* was measured at 280 nm by using a UV/Vis spectrophotometer (SP-890, Barnstead International). The column experiments were conducted at room temperature (22–25 °C).

The profile of retained *E. coli* O157:H7 cells in the column was determined after recovery of the breakthrough curve (BTC) using the procedure of Bradford et al. (2006b). The quartz sand was carefully excavated in 1 cm increments and placed into 50 mL tubes (Fisher Scientific) containing approximately 4 mL of the same electrolyte solution used for column experiments. The tubes were gently shaken for approximately 3 min by hand, and the supernatant collected and analyzed to determine the intensity of cell fluorescence using a Turner Quantech Fluorometer (FM109545, Barnstead International, Dubuque, IA). In this case, the fluorometer was used instead of a UV/Vis spectrophotometer to reduce background interference that originates from sand when using the spectrophotometer. With the fluorometer, the impact of this background interference was always less than 1%. The fluorometer has a fluorescent filter set with excitation and emission wavelengths of 490 and 515 nm to match the fluorescence of the *E. coli* O157:H7/pGFP strain. The concentration of the supernatant was determined from the sample fluorescence value via a concentration vs. fluorescence calibration curve. A new calibration curve was established for every experiment. The electrolyte volume and quartz mass in each tube was determined from a mass balance (samples were weighed before and after oven drying the sample overnight at 130 °C). In this work

Table 2 – Electrokinetic properties of quartz sand and *E. coli* O157:H7 cells as well as the height of energy barrier determined from DLVO interaction calculation.[a]

Ionic strength (mM)	Quartz surface potential (mV)	Outer surface potential[b] of *E. coli* O157:H7 (mV)		Energy barrier height (*kT*) for cell–quartz interaction		Energy barrier height (*kT*) for cell–cell interaction	
		Untreated	Proteinase K Treated	Untreated	Proteinase K Treated	Untreated	Proteinase K Treated
0.01	−68.2	−27.7	−73.1	512.9	2423.3	363.4	2609.7
0.1	−66.7	−3.73	−23.0	9.8	338.9	3.7	227.0
1	−51.6[c]	−0.375	−2.86	NB[d]	5.0	NB	NB
100	−13.1[c]	−0.004	−0.029	NB	NB	NB	NB

a The interaction energies were determined from the sum of retarded van der Waals interaction and electrical double layer interaction energies. Sphere–plate and sphere–sphere models were used to calculate the cell–quartz and cell–cell interaction energies, respectively. The values of 6.5×10^{-21} and 7.5×10^{-21} J were chosen as Hamaker constants for bacterium–water–quartz (A_{132}) and bacterium–water–bacterium (A_{131}), respectively.

b Value converted from experimentally measured electrophoretic mobility in Table 1 based on Ohshima's soft particle theory (Ohshima, 1994, 1995).

c Values from Kim et al. (2009a).

d No Energy Barrier.

the total mass balance is given as $100 = M_{rec} + M_{irrev}$, where M_{rec} and M_{irrev} denote the percentage of injected cells that are recovered and irreversibly retained in the column, respectively. The value of $M_{rec} = M_{eff} + M_{DI} + M_{FI} + M_{sand}$, where M_{eff}, M_{DI}, and M_{FI} denote the percentage of injected cells that are recovered by integration of the BTC during the initial colloid transport phase, the DI water flush, and the flow interruption, respectively, and M_{sand} is the percentage obtained from column dissection. Hence, the percentage of injected cells that are retained in the column is given as $M_{DI} + M_{FI} + M_{sand} + M_{irrev}$, the reversibly retained cells is given as $M_{DI} + M_{FI} + M_{sand}$, and the irreversibly retained cells is given as $M_{irrev} = 100 - M_{rec}$. The validity of this approach was confirmed by the relatively good mass balance results (M_{rec} equaled 100.3–109.5%) obtained under highly unfavorable conditions (IS = 0.01 mM for untreated cells, and IS of 0.01 and 0.1 mM for treated cells).

2.6. Calculation of cell–cell and cell–quartz interaction energy profiles

DLVO theory was used to calculate the total cell–cell and cell–quartz interaction energy as a function of separation distance. Cell–cell interaction energy was determined by considering the cell–cell interaction with the sphere–sphere model, whereas cell–quartz interaction energy was calculated by considering the system using the sphere–plate model. Due to the presence of extracellular macromolecules on the cells, the EPM data (Table 1) was converted to the outer surface potential using Ohshima's soft particle theory (Ohshima, 1994, 1995). These outer surface potentials and measured zeta potentials for the sand surfaces (Table 2) were used to calculate cell–cell and cell–quartz interaction energy profiles based on DLVO theory.

The retarded van der Waals attractive interaction energies for sphere–sphere ($\Phi_{VDW\text{-}SS}$) and sphere–plate ($\Phi_{VDW\text{-}SP}$) systems were calculated using Equations (1) and (2), respectively (Gregory, 1981).

$$\Phi_{VDW\text{-}SS} = -\frac{A_{131}a_{P1}a_{P2}}{6h(a_{P1}+a_{P2})}\left[1-\frac{5.32h}{\lambda}\ln\left(1+\frac{\lambda}{5.32h}\right)\right]^{-1} \quad (1)$$

$$\Phi_{VDW-SP} = -\left\{\frac{A_{132}a_P}{6h}\right\}\left[1+\left(\frac{14h}{\lambda}\right)\right]^{-1} \quad (2)$$

Here a_{P1} and a_{P2} are the radii of two interacting cells, and h is the separation distance, a_P is the radius of the cell interacting with quartz surface, λ is the characteristic wavelength (usually taken as 100 nm), A is the Hamaker constant. The subscripts 1, 2, and 3 on A denote bacterium, quartz, and water, respectively. The A_{132} value of 6.5×10^{-21} J was adopted from Redman et al. (2004). The value of A_{131} was estimated to be 7.5×10^{-20} J based on the geometrical mean assumption for Hamaker constants (van Oss, 1994), and assuming 8.4×10^{-20} and 4.6×10^{-20} J for A_{22} and A_{33} components, respectively (Israelachvili, 1992; Visser, 1972).

The electrical double layer interaction energies for sphere–sphere ($\Phi_{EDL\text{-}SS}$) and sphere–plate ($\Phi_{EDL\text{-}SP}$) systems were calculated using Equations (3) and (4), respectively (Hogg et al., 1966).

$$\Phi_{EDL-SS} = \frac{2\pi a_{P1}a_{P2}n_\infty kT}{(a_{P1}+a_{P2})\kappa^2}(\varphi_{P1}^2+\varphi_{P1}^2)\left\{\frac{2\varphi_{P1}\varphi_{P2}}{\varphi_{P1}^2+\varphi_{P2}^2}\ln\left[\frac{1+\exp(-\kappa h)}{1-\exp(-\kappa h)}\right] + \ln[1-\exp(-2\kappa h)]\right\} \quad (3)$$

$$\Phi_{EDL-SP} = \pi\varepsilon_0\varepsilon_r a_P\left\{2\psi_P\psi_C\ln\left[\frac{1+\exp(-\kappa h)}{1-\exp(-\kappa h)}\right] + (\psi_P^2+\psi_C^2)\ln[1-\exp(-2\kappa h)]\right\} \quad (4)$$

Here n_∞ denotes the bulk number density of ions (N m^{-3}, where N is the number), k is the Boltzmann constant (J K^{-1}), T the absolute temperature of the system (K), φ_{P1} and φ_{P2} are the reduced potentials ($\varphi = ze\psi/kT$) of two interacting cells (dimensionless), ψ_P and ψ_C are the electric potentials of the cell and the quartz (V), z is the ion valence (dimensionless), e the electron charge (C), ε_0 the permittivity of vacuum (C V^{-1} m^{-1}), ε_r the relative permittivity of water (dimensionless), and κ represents the Debye–Hückel reciprocal length (m^{-1}). The value of κ can be determined by

$$\kappa = \sqrt{\left(\frac{e^2\sum n_{i0}z_i^2}{\varepsilon_0\varepsilon_r kT}\right)} \quad (5)$$

Here n_{i0} and z_i represent number concentration and valence of ion i in bulk solution, respectively.

3. Results and discussion

3.1. Electrokinetic property of untreated and proteinase K treated E. coli O157:H7

The EPM for untreated cells ranged from −1.23 to −0.11 (μm/sec)/(V/cm) when the IS ranged from 0.01 to 100 mM KCl and the pH was 5.8. In contrast, the EPM of the proteinase K treated cells ranged from −3.09 to −0.05 (μm/sec)/(V/cm) over these same solution chemistry conditions (Table 1). This observation indicates that the extracellular macromolecules may shift the position of the shear plane away from the cell surface and diminish the surface potential of *E. coli* O157:H7 cells as suggested by Elimelech et al. (1995). It should be mentioned that differences in the EPM of untreated and proteinase K treated cells were most pronounced for IS ≤ 1 mM ($P < 0.05$), whereas no statistical difference ($P > 0.05$) was observed for IS of 100 mM.

3.2. Cell–cell and cell–quartz interaction energies

Table 2 presents results for cell–cell and cell–quartz interaction energy calculations for both untreated and proteinase K treated cells. No energy barrier occurs between cells and sand surface when the IS ≥ 1 mM, indicating that similar transport behavior is expected for both untreated and treated cells under these conditions. Hence, our subsequent studies discussed below for the proteinase K treated cells were only conducted at IS of 0.1 and 0.01 mM.

Fig. 1A and B show the cell–quartz and cell–cell DLVO interaction energy profiles, respectively, for untreated cells. Increasing the IS compressed the diffuse double layer outside

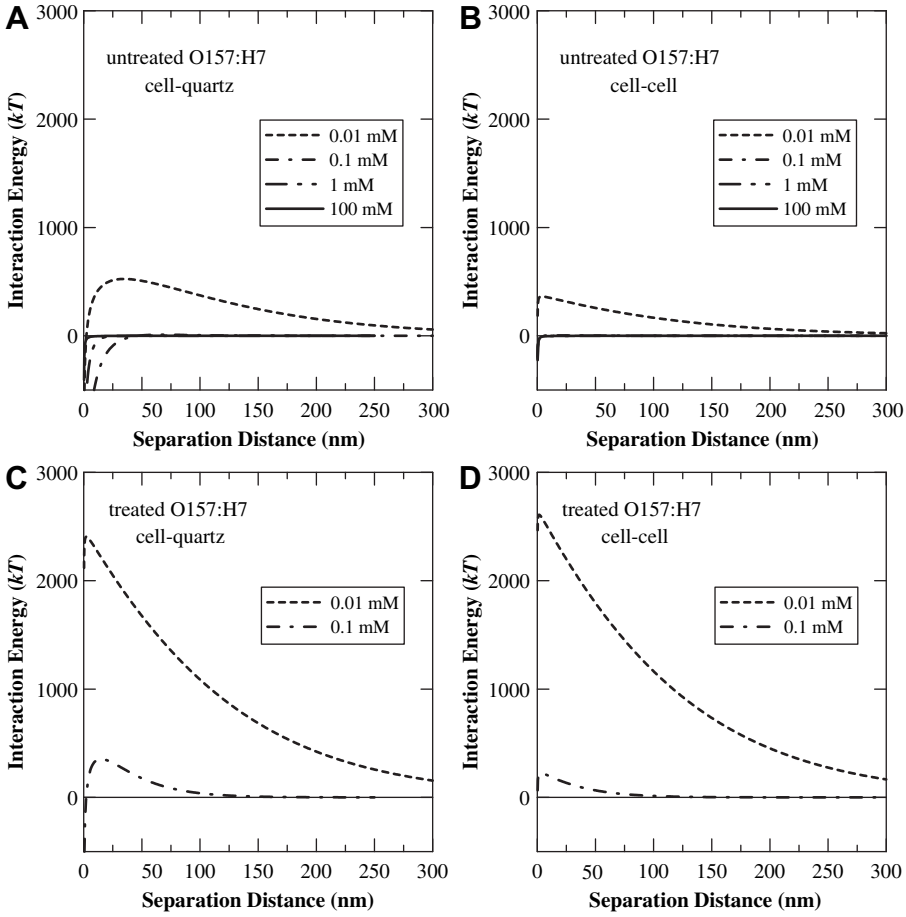

Fig. 1 – Cell–quartz and cell–cell interaction energy profiles for untreated (A and B) and proteinase K treated (C and D) *E. coli* O157:H7 cells as a function of separation distance at different solution IS. Surface potentials of *E. coli* O157:H7 and quartz given in Table 2 were used for the calculation. Bacterial cell sizes used in calculations are adapted from Kim et al. (2009b).

the surface of the cells and the quartz sand, and subsequently caused a decrease in the electrostatic repulsive force between the two surfaces. No energy barrier exists for cell–quartz and cell–cell interactions for IS $\geq$ 1 mM, indicating that the interacting conditions are favorable for cell attachment to quartz and to other cells. On the other hand, the interaction energy profiles show an energy barrier to cell attachment to quartz and to other cells at IS = 0.1 mM (9.8 and 3.7 kT for cell–quartz and cell–cell interactions, respectively) and IS = 0.01 mM (512.9 and 363.4 kT for cell–quartz and cell–cell interactions, respectively), and no secondary energy minimum. These observations indicate highly unfavorable conditions for *E. coli* O157:H7 deposition to the quartz and for cell–cell interactions when the IS $\leq$ 0.1 mM.

Fig. 1C and D show the cell–quartz and cell–cell DLVO interaction energy profiles, respectively, for the proteinase K treated cells for IS of 0.1 and 0.01 mM. Similarly to the untreated cells, the interaction energy profiles indicate unfavorable conditions for cell–quartz and cell–cell interactions at these IS. However, much larger energy barriers are predicted for proteinase K treated cells than untreated cells. Specifically, an enormous energy barrier exists for cell–quartz and cell–cell interactions at IS = 0.1 mM for the treated cells (338.9 and 227.0 kT for cell–quartz and cell–cell interactions, respectively) as compared to the untreated cells (9.8 and 3.7 kT for cell–quartz and cell–cell interactions, respectively). At an IS of 0.01 mM the energy barrier to cell–quartz and cell–cell interactions was very unfavorable for both untreated and treated cells (>363 kT).

3.3. *Cell aggregation*

The results of aggregation experiments (average of three replicates) with untreated cells are presented in Fig. 2. Increasing the IS led to faster cell aggregation as suggested by a steeper slope. This is due to cell–cell aggregates forming and settling out of suspension. The average first-order aggregation rate constants (k) obtained from the data for the untreated cells were determined to be 8.8×10^{-3}, 1.3×10^{-2}, 2.3×10^{-2}, 5.6×10^{-2} h^{-1} at IS of 0.01, 0.1, 1, and 100 mM KCl, respectively (Table 3). The cell aggregation rate at IS of 0.1, 1, and 100 mM is approximately 1.5, 2.6, and 6.4 times greater than that at IS = 0.01 mM. The fact that cell aggregation rates increase with IS supports the possibility of cell–cell interactions, and is qualitatively consistent with the predicted trend of cell–cell interactions shown in Fig. 1B.

Average cell aggregation results for proteinase K treated cells at IS of 0.1 and 0.01 mM are also shown in Fig. 2. Similar with the result for the untreated cells, increasing the IS led to slightly faster cell aggregation rates (Table 3); however, the

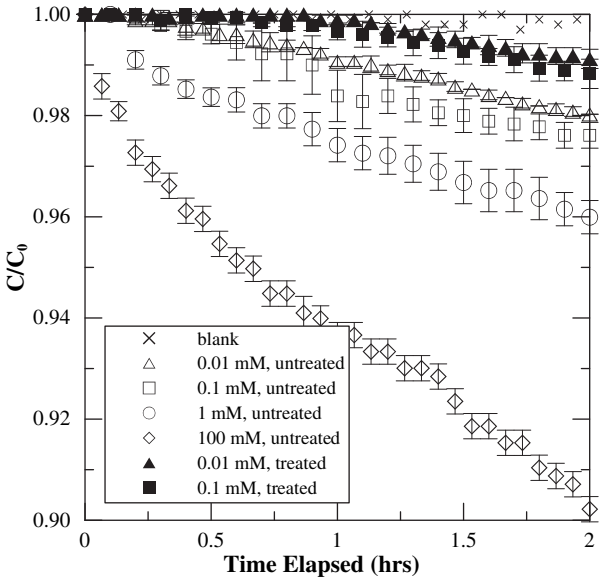

Fig. 2 – Relative concentration vs. time for untreated (open) and proteinase K treated (solid) *E. coli* O157:H7 cells. Experiments were carried out at pH 5.8 and at room temperature (22–25 °C). Error bars indicate one standard deviation.

difference was not statistically significant ($P > 0.05$). The aggregation rate for the treated cells (3.3×10^{-3} and 4.8×10^{-3} h^{-1} at IS of 0.01 and 0.1 mM, respectively) is lower than the untreated cells (8.8×10^{-3} and 1.3×10^{-2} h^{-1} at IS of 0.01 and 0.1 mM, respectively) at the same IS conditions. This observation suggests that macromolecules on the untreated cells may still be weakly interacting even at an IS of 0.1 and 0.01 mM and enhancing cell–cell interaction.

3.4. *Transport and retention behavior of untreated E. coli O157:H7*

Fig. 3 shows BTCs (Fig. 3A) and retention profiles (Fig. 3B) for untreated *E. coli* O157:H7 cells at IS of 0.01, 0.1, 1, and 100 mM KCl. Mass balance information was determined from these BTCs and the cell retention profiles, and the results are summarized in Table 4. The quantity of cells recovered in the column effluent (M_{eff}) tended to decrease with increasing IS (84.7, 9.3, 0.9, and 1.9% of total injected mass at IS of 0.01, 0.1, 1, and 100 mM KCl, respectively), and the concentration of retained cells correspondingly increases with IS. Differences in the cell retention profiles between IS of 1 and 100 mM systems shown in Fig. 3B is due to the loss of the cells eluted by two additional steps (i.e., flow interruption and DI water flush) after recovery of the BTC in the IS = 1 mM system. Note that no flow interruption and DI water flush tests were carried out for the IS = 100 mM system. Overall, the transport and retention behavior is conceptually consistent with the DLVO profile presented in Fig. 1, in that increasing the IS allowed more cells to be retained in the column (Fig. 3A and Table 4) as observed from other studies (Elimelech et al., 1995; Redman et al., 2004). A close examination of this data, however, reveals some discrepancies with DLVO predictions, which are discussed below.

Table 3 – Average first-order aggregation rate constants (k) and coefficients of linear regression values (r^2) for untreated and proteinase K treated *E. coli* O157:H7 cells as a function of IS.[a]

Ionic strength (mM)	Untreated		Proteinase K treated	
	k (h^{-1})	r^2	k (h^{-1})	r^2
0.01	$8.8 \times 10^{-3} \pm 1.0 \times 10^{-3}$	0.985	$3.3 \times 10^{-3} \pm 7.7 \times 10^{-4}$	0.833
0.1	$1.3 \times 10^{-2} \pm 1.8 \times 10^{-3}$	0.967	$4.8 \times 10^{-3} \pm 1.4 \times 10^{-3}$	0.918
1	$2.3 \times 10^{-2} \pm 2.3 \times 10^{-3}$	0.983	ND	ND
100	$5.6 \times 10^{-2} \pm 2.1 \times 10^{-3}$	0.974	ND	ND

a The values were determined by fitting first-order kinetic equation to the experimentally measured data in Fig. 2. ND Not determined.

The DLVO interaction energy profiles presented in Fig. 1A and B predict that cell–quartz and cell–cell interactions are favorable when IS ≥ 1 mM, slightly unfavorable when IS = 0.1 mM, and very unfavorable when IS = 0.01 mM. Favorable conditions imply irreversible attachment in the primary minimum. Consistent with this prediction, almost 100% of the injected cells were retained in the column when the IS was ≥1 mM (Fig. 3A). In contrast, mass balance results shown in Table 4 indicate that the percent of cells reversibly retained in the column ($M_{sand} + M_{FI} + M_{DI}$) increased with increasing IS (conversely, 40.7, 40.7, and 45.1, and 0% of the injected cells were irreversibly retained in the systems with IS of 100, 1, 0.1, and 0.01 mM, respectively). It therefore appears that similar amounts of irreversibly retained cells occurred when IS ≥ 0.1 mM. Under favorable attachment conditions (IS of 1 and 100 mM shown in Fig. 1) irreversible attachment in the primary minimum is expected due to the absence of an energy barrier. Under slightly unfavorable attachment conditions (IS = 0.1 mM) it is possible for some of the cells to overcome the energy barrier (9 kT) to attachment in the primary minimum due to diffusion (Franchi and O'Melia, 2003) or chemical heterogeneity (Baygents et al., 1998; Walker et al., 2005).

Table 4 reports that 15.6, 45.6, 58.4 ($M_{sand} + M_{FI} + M_{DI}$ in this case), and 57.4% of the injected cells in the IS of 0.01, 0.1, 1, and 100 mM systems, respectively, were reversibly recovered from the sand after completion of the column experiments. The cells that can be recovered after DI water flush, flow interruption, or excavating the sand in the column are weakly associated with the solid phase. Interaction of the cells on the quartz surface by the secondary energy minimum is unlikely based on calculations presented in Fig. 1 and Table 2. Three factors can likely explain the reversible cell retention behavior, namely: (a) steric stabilization; (b) cell–cell interactions; and (c) funneling of weakly associated cells to the smallest regions of the pore space that are associated with lower hydrodynamic forces. Each of these hypotheses will be discussed below.

Steric stabilization of extracellular macromolecules can limit the approach distance of cells to the quartz surface (Elimelech et al., 1995; Israelachvili, 1992) and thereby hinder

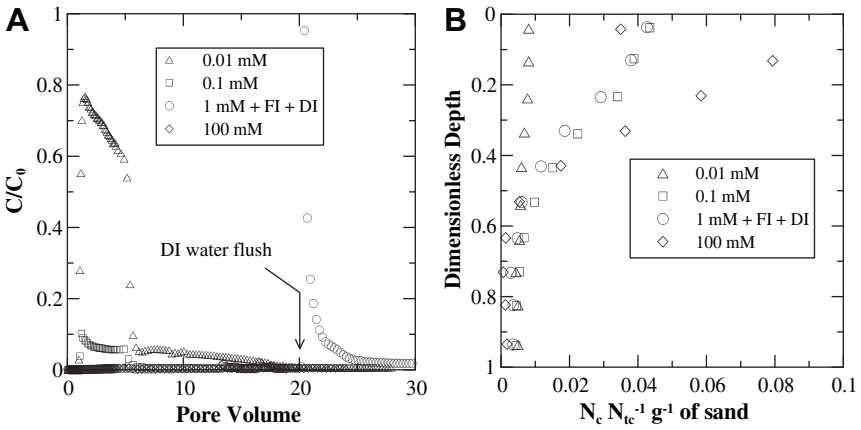

Fig. 3 – Breakthrough curves (A) and retention profiles (B) for untreated *E. coli* O157:H7 at different IS. In the legend, FI and DI denote flow interruption and DI water flush, respectively. In Fig. 3B, the deposition profile at IS = 1 mM was obtained after two consecutive flow interruptions (occurring at PV of 13.3 and 16.5, respectively) and the DI water flush. The X-axis represents the normalized concentration of the cells (the number of cells in each section, N_c, divided by the total number injected into the column, N_{tc}) per gram of dry sand. The breakthrough and retention profile data for IS of 1 and 100 mM were adapted from Kim et al. (2009a).

attachment in the primary minimum, even under favorable attachment conditions (IS = 1 and 100 mM). For example, Kuznar and Elimelech (2006) observed in an RSPF system that the attachment efficiency of *C. parvum* oocysts was much smaller than unity under favorable attachment conditions. These authors attributed this unusual deposition trend to electrosteric stabilization of the macromolecules on the oocyst surface. As mentioned in the introduction, they did not discuss the potential reversibility of retained oocysts by steric repulsion since the RSPF system only captures irreversible cell attachment (i.e., primary energy minimum interaction).

Table 4 – Mass balance results for untreated and proteinase K treated *E. coli* O157:H7 cells obtained from column experiments.[a]

Ionic strength (mM)	M_{eff} (%)	M_{FI} (%)	M_{DI} (%)	M_{sand} (%)	M_{rec} (%)	100 − M_{rec} (%)
Untreated *E. coli* O157:H7						
0.01	84.7	–	–	15.6	100.3	<0
0.1	9.3	–	–	45.6	54.9	45.1
1[b]	0.9	0.8[c]	18.7	38.9	59.3	40.7
100[b]	1.9	–	–	57.4	59.3	40.7
Proteinase K treated *E. coli* O157:H7						
0.01	100.3	1.1[d]	0.4	5.2	107.0	<0
0.1	89.7	1.7[d]	11.8	6.3	109.5	<0

a M_{eff}, M_{DI}, and M_{FI} denote the percentage of injected cells that are recovered by integration of the BTC during the initial colloid transport phase, the DI water flush, and the flow interruption, respectively, and M_{sand} is the percentage obtained from column dissection. M_{rec} represents the sum of all percentages (i.e., M_{eff}, M_{FI}, M_{DI}, and M_{sand}).
b Data from Kim et al. (2009a).
c Percent recovery of the injected cells eluted by 1st (~3.2 PV) and 2nd (~10.4 PV) flow interruption.
d Percent recovery of the injected cells eluted by flow interruption of 5.2 PV.

However, it is plausible that the addition of repulsive steric force to DLVO forces (i.e., sum of van der Waals attractive and electrostatic forces) may lead to the change in the total interaction energy and make the conditions more unfavorable (Hiemenz and Rajagopalan, 1997). Furthermore, the possibility of weak interaction between cells and surfaces (i.e., the existence of secondary energy minimum interaction) may be dependent on the magnitude of repulsive steric interaction (Hiemenz and Rajagopalan, 1997; Yoshioka et al., 1997). In addition to the cell–quartz steric stabilization, cell–cell steric stabilization could also contribute to the reversible cell retention observed under favorable conditions (i.e., 1 and 100 mM). In comparison to direct interaction of cells in the primary minima, steric stabilization produces weak cell–quartz or cell–cell interactions at a larger separation distance that is controlled by the extracellular macromolecule layer. Hence, steric stabilization of cells in the primary minima is expected to act in a similar way as cells associated with the secondary minima.

Fig. 1B indicates that cell–cell interactions are favorable in the IS of 1 and 100 mM systems, but unfavorable in the IS of 0.1 mM (3.7 *kT* energy barrier) and 0.01 mM (363.4 *kT* energy barrier) systems. The cell breakthrough results for the IS of 0.1 and 0.01 mM systems (Fig. 3A) show that the effluent concentrations in the plateau region of the BTCs decrease with time (i.e., ripening), indicating that cell–cell interactions are also likely involved in the cell retention mechanism (Bradford et al., 2007; Liu et al., 2008; Tong et al., 2008) under these conditions. The hypothesis that cell–cell interactions may be involved in cell retention processes is supported by results from the aggregation experiments shown in Fig. 2 and Table 3, as well as observations from a micromodel study (Kim et al., 2009a) that found that *E. coli* O157:H7 cells were preferentially attached to and coated specific sand grains under certain solution chemistry conditions. Furthermore, the cell retention profiles shown in Fig. 3B do not always decrease monotonically with depth (e.g., the greatest cell retention

occurred at a dimensionless depth of ca. 0.13 for the IS = 100 mM system). Such non-monotonic (bell-shaped) retention profiles are not consistent with the exponential decay in the amount of attached cells with distance predicted by classic filtration theory (Yao et al., 1971). These results suggest that the cells weakly associated with quartz surface or other cells by steric interaction may detach in the presence of hydrodynamic drag and subsequently be retained down-gradient. It should be noted that aggregated cells would be more vulnerable to hydrodynamic shear than a singe cell (Torkzaban et al., 2007). This hypothesis is supported by the results from Tong et al. (2005) and Bradford et al. (2006b). For example, Tong et al. (2005) observed non-monotonic retention profiles from a column study using *Comamonas* DA001 under favorable conditions. They also attributed the unusual shape of the retention profiles to weak interaction by steric repulsion as well as detachment of the cells due to hydrodynamic drag. These hypotheses were supported by the observed migration of the peak retained cell concentration down-gradient with increasing elution time and flow rate. Bradford et al. (2006b) also reported non-monotonic retention profiles under unfavorable conditions using the same *E. coli* O157:H7 strain used in this study. They attributed the non-monotonic retention profile to aggregation, breakage, and release of the cells in low velocity regions found near grain junctions, small pores, and pore constrictions. Potential explanations for cell–cell interactions in the IS of 0.1 and 0.01 mM systems include polymer bridging (Jucker et al., 1998; Liu et al., 2007, 2008) and biological cell–cell regulation (i.e., quorum sensing) (Parsek and Greenberg, 2000). Polymer bridging may occur under low IS conditions when the polymeric layers extend into the bulk solution (Abu-Lail and Camesano, 2003; Liu et al., 2007, 2008) and interact with high affinity surfaces (Liu et al., 2007). Indeed, the *E. coli* O157:H7 cells possess extracellular polymeric materials, and therefore polymer bridging interaction is plausible (Kim et al., 2009b). At the present, however, the exact mechanism for cell–cell interactions under these conditions is uncertain.

Many researchers have demonstrated that low velocity regions that are induced by the pore structure (e.g., grain junctions, small pore spaces, and pore constrictions) can enhance colloid/cell retention in porous media (Bradford et al., 2006b, 2007; Tong et al., 2008; Torkzaban et al., 2008) under unfavorable attachment conditions. In the present study, low velocity regions are also likely to be playing an important role in the retention of the *E. coli* O157:H7 cells. The result for IS = 1 mM, for instance, shows that a significant amount of the injected cells (M_{sand} = 38.9%) were still recovered from the column after conducting flow interruption and flushing the system with DI water. Recent literature has demonstrated that weakly associated cells and colloids in the secondary minimum may be funneled by hydrodynamic forces to regions that are associated with lower hydrodynamic forces and therefore enhanced retention (Bradford et al., 2007; Tong et al., 2008). Similarly, we hypothesize herein that cells weakly associated with the solid phase by steric stabilization may also be funneled to and retained in low velocity regions.

3.5. *Transport and retention behavior of proteinase K treated E. coli O157:H7*

Fig. 4 shows BTCs (Fig. 4A) and retention profiles (Fig. 4B) for proteinase K treated *E. coli* O157:H7 cells when the IS was 0.01 and 0.1 mM. Similar to the BTC results for untreated *E. coli* O157:H7 cells (Fig. 3A), more cells were retained in the column as IS increases (i.e., cell breakthrough of 100.3 and 89.7% of the injected cells in IS of 0.01 and 0.1 mM systems, respectively). A significantly smaller amount of the proteinase K treated cells were retained in the column as compared to the untreated ones (Table 4), indicating that the extracellular macromolecules of *E. coli* O157:H7 cells enhance the cell retention. The notably different cell retention between the proteinase K treated and untreated cells (IS = 0.1 mM) is due to electrostatic interactions of the untreated (9.8 kT) being much less than the proteinase K treated (338.9 kT) cells (Fig. 1 and Table 2). Cell–cell interactions were also diminished by the

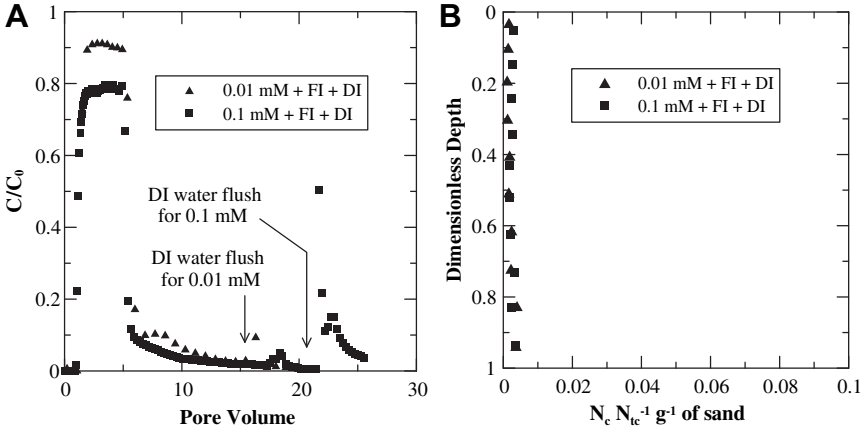

Fig. 4 – Breakthrough curves (A) and retention profiles (B) for proteinase K treated *E. coli* O157:H7 cells at different IS. In the legend, FI and DI denote flow interruption and DI water flush, respectively. The cell deposition profiles in Fig. 4B were obtained after a flow interruption and DI water flush. The X-axis represents the normalized concentration of the cells (the number of cells in each section, N_c, divided by the total number injected into the column, N_{tc}) per gram of dry sand.

removal of the extracellular macromolecules on the *E. coli* O157:H7 cells. This conclusion is supported by the difference in the DLVO interaction energies (Fig. 1B and D), the cell aggregation results (Fig. 2 and Table 3), and differences in the shape of the BTC for untreated (Fig. 3A) and proteinase K treated cells (Fig. 4A). In particular, notice that the BTC for proteinase K treated cells (Fig. 4A) does not exhibit ripening that occurred for the untreated cells (Fig. 3A).

The cell–quartz interaction energy shown in Fig. 1C indicates that conditions are highly unfavorable for irreversible cell attachment in the primary minimum (height of energy barrier = 2423.3 and 338.9 kT at 0.01 and 0.1 mM, respectively) and no secondary energy minimum was present. However, mass balance results presented in Table 4 show that reversible retention of the treated cells occurred in the 0.01 and 0.1 mM systems. Plausible mechanisms for the reversible cell retention under these conditions include interaction by polymer bridging (Jucker et al., 1998; Liu et al., 2007, 2008) and retention induced by the pore structure and/or the quartz surface roughness (Bradford et al., 2006a,b, 2007; Tufenkji and Elimelech, 2004; Tufenkji et al., 2004). Mass balance results show that approximately 11.8% of the injected cells (M_{DI}) were eluted by switching the electrolyte to DI water in the IS = 0.1 mM system, indicating the presence of a weak cell–quartz interaction. Here, it should be noted that the treated cells may still possess polysaccharide chains, which are not linked with protein structure and may cause cell retention to some extent, since proteinase K cleaves the macromolecules associated with protein structure (Kuznar and Elimelech, 2006; Kim et al., 2009b). The fact that the reversible cell retention is likely due to the polymer bridging interaction can also be supported by the tailing behavior observed in the BTC for the IS = 0.1 mM system. In particular, notice that only 1.7% (M_{FI}) of the injected cells were released by flow interruption, whereas 11.8% (M_{DI}) were released by flushing with DI water. If the tailing was controlled by cell diffusion, then the flow interruption test results would have shown larger amounts of cell release. The results indicate that the tailing is likely associated with the detachment of the cells due to the hydrodynamic shear force (Li et al., 2005; Bradford et al., 2007; Liu and Li, 2008), which may otherwise be weakly attached to the quartz surface by polymer bridging. It should be noted that even after DI water flushing, approximately 5.2 and 6.3% of the injected cells (M_{sand}) were reversibly recovered from the quartz sand at IS of 0.01 and 0.1 mM, respectively. This retention likely occurred as a result of the pore structure and/or surface roughness, which may serve as hydrodynamically favorable regions for cell retention (Vaidyanathan and Tien, 1988; Torkzaban et al., 2008).

4. Conclusions and implications

Comparison of the transport and retention behavior between macromolecule rich and deficient cells indicate that pathogenic *E. coli* O157:H7 retention in saturated porous media can be significantly influenced by macromolecule-mediated interactions. It was found that the macromolecule-related interactions are strongly linked to solution IS. Classic DLVO theory, which does not account for macromolecule-mediated interactions such as polymer bridging or steric repulsion, was found to be insufficient to accurately predict the retention of *E. coli* O157:H7 cells in porous media. Evidence to this effect was the fact that a significant amount of cells were retained under unfavorable conditions with no secondary energy minimum, and irreversible cell retention was hindered under favorable conditions.

Significantly enhanced retention with time (i.e., ripening) and a faster aggregation rate for untreated cells suggests that cell–cell and cell–quartz interactions are also important mechanisms for the retention of *E. coli* O157:H7 cells in porous media. Furthermore, the non-monotonic cell retention profile under favorable conditions, which deviates from classic filtration theory, indicates that cells may be weakly associated with other cells or quartz surface due to steric interactions and susceptible to removal by hydrodynamic forces. Both of these processes are commonly neglected in classical theories of cell interaction and retention. Caution is therefore warranted in predicting the travel distance of pathogens in (drinking or riverbank) water filtration facilities using current theoretical models. For example, neglecting cell–cell interactions and steric interactions in travel distance predictions may lead to an overestimation and underestimation, respectively. Furthermore, biofilm formation developed by cell–cell interactions might cause significant costs in long-term operation of treatment systems.

Acknowledgements

This research was funded by the USDA CSREES NRI (Grant #: 2006-02541). Permission from the American Chemical Society to use the electrophoretic mobility data (Kim et al., 2009b) that is presented in Table 1 is gratefully acknowledged. The breakthrough and retention profile data for IS of 1 and 100 mM systems (Kim et al., 2009a) shown in Fig. 3 is used with kind permission of Springer Science and Business Media.

REFERENCES

Abu-Lail, N.I., Camesano, T.A., 2003. Role of ionic strength on the relationship of biopolymer conformation, DLVO contributions, and steric interactions to bioadhesion of *Pseudomonas putida* KT2442. Biomacromolecules 4, 1000–1012.

Baygents, J.C., Glynn Jr., J.R., Albinger, O., Biesemeyer, B.K., Ogden, K.L., Arnold, R.G., 1998. Variation of surface charge density in monoclonal bacterial populations: implications for transport through porous media. Environ. Sci. Technol. 32, 1596–1603.

Boulos, L., Prevost, M., Barbeau, B., Coallier, J., Desjardins, R., 1999. LIVE/DEAD BacLight: application of a new rapid staining method for direct enumeration of viable and total bacteria in drinking water. J. Microbiol. Meth. 37, 77–86.

Boyce, T.G., Swerdlow, D.L., Griffin, P.M., 1995. Current concepts: *Escherichia coli O157:H7* and the hemolytic-uremic syndrome. N. Engl. J. Med. 333, 364–368.

Bradford, S.A., Simunek, J., Battahar, M., van Genuchten, M.T., Yates, S.R., 2006a. Significance of straining in colloid deposition: evidence and implications. Water Resour. Res. 42, W12S15.

Bradford, S.A., Simunek, J., Walker, S.L., 2006b. Transport and straining of *E. coli O157:H* in saturated porous media. Water Resour. Res. 42, W12S12. doi:10.1029/2005WR004805.

Bradford, S.A., Torkzaban, S., Walker, S.L., 2007. Coupling of physical and chemical mechanisms of colloid straining in saturated porous media. Water Res. 41, 3012–3024.

Chen, G., Walker, S.L., 2007. The role of solution chemistry and ion valence on the adhesion kinetics of groundwater and marine bacteria. Langmuir 2 (3), 7162–7169.

Dean-Nystrom, E.A., Melton-Celsa, A.R., Pohlenz, J.F.L., Moon, H.W., O'Brien, A.D., 2003. Comparative pathogenicity of *Escherichia coli* O157 and intimin-negative non-O157 shiga toxin-producing *E. coli* strains in neonatal pigs. Infect. Immun. 71, 6526–6533.

Derjaguin, B.V., Landau, L.D., 1941. Theory of stability of highly charged lyophobic sols and adhesion of highly charged particles in solutions of electrolytes. Acta Physicochim. USSR 14, 633–662.

Elimelech, M., Gregory, J., Jia, X., Williams, R.A., 1995. Particle Deposition and Aggregation: Measurement, Modeling and Simulation. Butterworth-Heinemann, Oxford, England.

Frank, J.F., 2001. Microbial attachment to food and food contact surfaces. Adv. Food Nutr. Res. 43, 320–370.

Franchi, A., O'Melia, C.R., 2003. Effects of natural organic matter and solution chemistry on the deposition and reentrainment of colloids in porous media. Environ. Sci. Technol. 37, 1122–1129.

Gargiulo, G., Bradford, S.A., Simunek, J., Ustohal, P., Vereecken, H., Klumpp, E., 2007. Bacteria transport and deposition under unsaturated conditions: the role of the matrix grain size and the bacteria surface protein. J. Contam. Hydrol. 92, 255–273.

Ginn, T.R., Wood, B.D., Nelson, K.E., Schiebe, T.D., Murphy, E.M., Clement, T.P., 2002. Processes in microbial transport in the natural subsurface. Adv. Water Res. 25, 1017–1042.

Gregory, J., 1981. Approximate expressions for retarded van der Waals interaction. J. Colloid Interface Sci. 83, 138–145.

Hiemenz, P.C., Rajagopalan, R., 1997. Principles of Colloid and Surface Chemistry, third ed. Marcel Dekker, New York.

Hogg, R.I., Healey, T.W., Fuerstenau, D.W., 1966. Mutual coagulation of colloidal dispersions. Trans. Faraday Soc. 62, 1638–1651.

Israelachvili, J.N., 1992. Intermolecular and Surface Forces. Academic Press, Amsterdam, Boston.

Jin, Y., Flury, M., 2002. Fate and transport of viruses in porous media. Adv. Agron. 77, 39–102.

Jucker, B.A., Zehnder, A.J.B., Harms, H., 1998. Quantification of polymer interactions in bacterial adhesion. Environ. Sci. Technol. 32, 2909–2915.

Kaper, J.B., Karmali, M.A., 2008. The continuing evolution of a bacterial pathogen. Proc. Natl. Acad. Sci. 105 (12), 4535–4536.

Kim, H.N., Bradford, S.A., Walker, S.L., 2009a. *Escherichia coli* O157:H7 transport in saturated porous media: role of solution chemistry and surface macromolecules. Environ. Sci. Technol. 43, 4340–4347.

Kim, H.N., Hong, Y., Lee, I., Bradford, S.A., Walker, S.L., 2009b. Surface characteristics and adhesion behavior of *Escherichia coli* O157:H7: role of extracellular macromolecules. Biomacromolecules 10, 2556–2564.

Kuznar, Z.A., Elimelech, M., 2005. Role of surface proteins in the deposition kinetics of *Cryptosporidium parvum* oocysts. Langmuir 21, 710–716.

Kuznar, Z.A., Elimelech, M., 2006. *Cryptosporidium* oocyst surface macromolecules significantly hinder oocyst attachment. Environ. Sci. Technol. 40, 1837–1842.

Kuznar, Z.A., Elimelech, M., 2007. Direct microscopic observation of particle deposition in porous media: role of the secondary energy minimum. Colloid Surf. Physicochem. Eng. Aspect. 294, 156–162.

Law, D.J., 2000. Virulence factors of *Escherichia coli* O157 and other Shiga toxin-producing *E. coli*. J. Appl. Microbiol. 88, 729–745.

Li, X., Zhang, P., Lin, C.L., Johnson, W.P., 2005. Role of hydrodynamic drag on microsphere deposition and re-entrainment in porous media under unfavorable conditions. Environ. Sci. Technol. 39, 4012–4020.

Litton, G.M., Olson, T.M., 1993. Colloid deposition rates on silica bed media and artifacts related to collector surface preparation methods. Environ. Sci. Technol. 27, 185–193.

Liu, Y., Yang, C.H., Li, J., 2007. Influence of extracellular polymeric substances on *Pseudomonas aeruginosa* transport and deposition profiles in porous media. Environ. Sci. Technol 41, 198–205.

Liu, Y., Li, J., 2008. Role of *Pseudomonas aeruginosa* biofilm in the initial adhesion, growth and detachment of *Escherichia coli* in porous media. Environ. Sci. Technol. 42, 443–449.

Liu, Y., Yang, C.-H., Li, J., 2008. Adhesion and retention of a bacterial phytopathogen *Erwinia chrysanthemi* in biofilm-coated porous media. Environ. Sci. Technol. 42, 159–165.

Mead, P.S., Slutsker, L., Dietz, V., McCaig, L.F., Bresee, J.S., Shapiro, C., Griffin, P.M., Tauxe, R.V., 1999. Food-related illness and death in the United States. Emerg. Infect. Dis. 5, 607–625.

Oh, Y.J., Jo, W., Yang, Y., Park, S., 2007. Influence of culture conditions on *Escherichia coli* O157:H7 biofilm formation by atomic force microscopy. Ultramicroscopy 107, 869–874.

Ohshima, J., 1994. Electrophoretic mobility of soft particles. J. Colloid Interface Sci. 163, 474–483.

Ohshima, H., 1995. Electrophoretic mobility of soft particles. Colloid Surf. Physicochem. Eng. Aspect. 103, 249–255.

Parsek, M.R., Greenberg, E.P., 2000. Acyl-homoserin lactone quorum sensing in Gram-negative bacteria: a signaling mechanism involved in association with higher organisms. Proc. Natl. Acad. Sci. 97, 8789–8793.

Pembrey, R.S., Marshall, K.C., Schneider, R.P., 1999. Cell surface analysis techniques: what do cell preparation protocols do to cell surface properties? Appl. Environ. Microbiol. 65, 2877–2894.

Redman, J.A., Walker, S.L., Elimelech, M., 2004. Bacterial adhesion and transport in porous media: role of the secondary energy minimum. Environ. Sci. Technol. 38, 1777–1785.

Rijnaarts, H.H.M., Norde, W., Lyklema, J., Zehnder, A.J.B., 1999. DLVO and steric contributions to bacterial deposition in media of different ionic strengths. Colloid Surf. B: Biointerfaces 14, 179–195.

Ryu, J.-H., Beuchat, L.R., 2005. Biofilm formation by *Escherichia coli* O157:H7 on stainless steel: effect of exopolysaccharide and curli production on its resistance to chlorine. Appl. Environ. Microbiol. 71, 247–254.

Schijven, J.K., Hassanizadeh, S.M., 2000. Removal of viruses by soil passage: overview of modeling, processes, and parameters. Crit. Rev. Environ. Sci. Technol. 30, 49–127.

Seltmann, G., Holst, O., 2002. The Bacterial Cell Wall. Springer, Berlin, New York.

Shen, C., Li, B., Huang, Y., Jin, Y., 2007. Kinetics of coupled primary- and secondary-minimum deposition of colloids under unfavorable chemical conditions. Environ. Sci. Technol. 41, 6976–6982.

Tong, M., Li, X., Brow, C.N., Johnson, W.P., 2005. Detachment-influenced transport of an adhesion-deficient bacterial strain within water-reactive porous media. Environ. Sci. Technol. 39, 2500–2508.

Tong, M., Ma, H., Johnson, W.P., 2008. Funneling of flow into grain-to-grain contacts drives colloid-colloid aggregation in the presence of an energy barrier. Environ. Sci. Technol. 42, 2826–2832.

Torkzaban, S., Bradford, S.A., Walker, S.L., 2007. Resolving the coupled effects of hydrodynamics and DLVO forces on colloid attachment in porous media. Langmuir 23, 9652–9660.

Torkzaban, S., Tazehkand, S.S., Walker, S.L., Bradford, S.A., 2008. Transport and fate of bacteria in porous media: coupled effects of chemical conditions and pore space geometry. Water Resour. Res. 44, W04403. doi:04410.01029/02007WR006541.

Tufenkji, N., Elimelech, M., 2004. Deviation from classical colloid filtration theory in the presence of repulsive DLVO interactions. Langmuir 20, 10818–10828.

Tufenkji, N., Miller, G.F., Ryan, J.N., Harvey, R.W., Elimelech, M., 2004. Transport of *Cryptosporidium* oocysts in porous media: role of straining and physicochemical filtration. Environ. Sci. Technol. 38, 5932–5938.

Vaidyanathan, R., Tien, C., 1988. Hydrosol deposition in granular beds. Chem. Eng. Sci. 43, 289–302.

van Oss, C.J., 1994. Interfacial Forces in Aqueous Media. Marcel Dekker, New York.

Verwey, E.J.W., Overbeek, J.T.G., 1948. Theory of the Stability of Lyophobic Colloids. Elsevier, Amsterdam.

Visser, J., 1972. On Hamaker constants: a comparison between Hamaker constants and Lifshitz–van der Waals constants. Adv. Colloid Interface Sci. 3, 331–363.

Voloshin, S.A., Kaprelyants, A.S., 2004. Cell–cell interactions in bacterial populations. Biochemistry (Mosc) 69, 1268–1275.

Walker, S.L., Redman, J.A., Elimelech, M., 2005. Influence of growth phase on bacterial deposition: interaction mechanism in packed bed column and radial stagnation point flow systems. Environ. Sci. Technol. 39, 6405–6411.

Wingender, J., Neu, T.R., Flemming, H.C., 1999. Microbial Extracellular Polymeric Substances. Springer, Berlin.

Yao, K.M., Habibian, M.T., O'Melia, C.R., 1971. Water and wastewater treatment filtration: concepts and applications. Environ. Sci. Technol. 5, 1105–1112.

Yoshioka, K., Sakai, E., Daimon, M., Kitahara, A., 1997. Role of steric hindrance in the performance of superplasticizers for concrete. J. Am. Ceram. Soc. 80, 2667–2771.